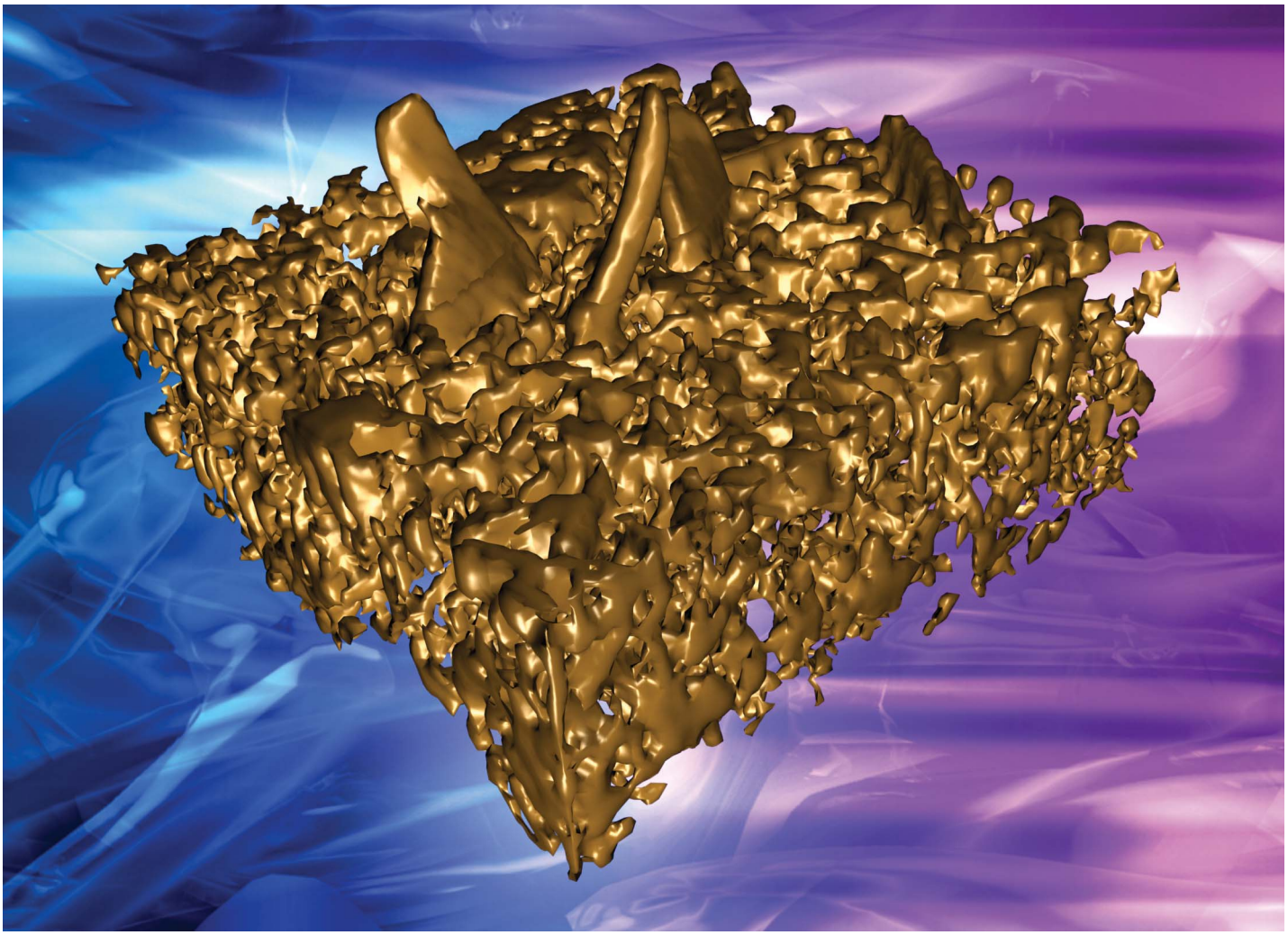

**A 3D computer model derived from the TEM tomogram of an organic solar cell active layer, highlighting research results from Bio21 Institute, School of Chemistry, the University of Melbourne, Australia.**

Title: The role of solvent vapor annealing in highly efficient air-processed small molecule solar cells

Rapid solvent vapor annealing performed in air changes the absorption profile, morphology and charge transport properties of the active layer consisting of a small molecule donor and a fullerene derivative, leading to excellent photovoltaic performance. A range of solvents has been tested, and selection rules are proposed for the enhancement of organic solar cell device performance.

## As featured in:

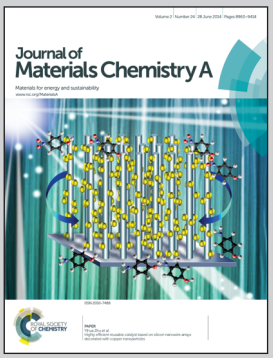


See Kuan Sun, Wallace W. H. Wong, David J. Jones *et al.*, *J. Mater. Chem. A*, 2014, **2**, 9048.

ROYAL SOCIETY OF CHEMISTRY

www.rsc.org/MaterialsA

Registered charity number: 207890

Journal of Materials Chemistry A

PAPER

View Article Online
View Journal | View Issue



Cite this: J. Mater. Chem. A, 2014, 2, 9048

# The role of solvent vapor annealing in highly efficient air-processed small molecule solar cells†

Kuan Sun,*[a] Zeyun Xiao,[a] Eric Hanssen,[b] Michael F. G. Klein,[a] Henk H. Dam,[a] Marina Pfaff,[c] Dagmar Gerthsen,[c] Wallace W. H. Wong*[a] and David J. Jones*[a]

Received 6th March 2014
Accepted 17th March 2014

DOI: 10.1039/c4ta01125b

www.rsc.org/MaterialsA

We demonstrate highly-efficient, solution-processed small molecule solar cells with the best power conversion efficiency (PCE) of more than 5%. The active layer consists of a diketopyrrolopyrrole-based donor molecule (DPP(TBFu)$_2$) and a fullerene derivative ($PC_{71}BM$) that is spin cast and subsequently treated with solvent vapor annealing (SVA) in air. We find not all solvent vapors lead to the best PCE. Solvents of high vapor pressures and medium donor solubilities, such as tetrahydrofuran or carbon disulfide, are most suitable for SVA in the context of organic solar cell application. On the other hand, acceptor solubility plays an insignificant role in such a treatment. An active layer treated with ideal solvent vapors develops desirable phase separation in both lateral and vertical directions, as revealed by AFM, TEM and TEM tomography. The SVA also leads to enhanced hole mobility. We believe the fast SVA treatment performed in air is a viable way to tune the active layer morphology for printed solar cells.

## 1. Introduction

Organic photovoltaics (OPVs) based on the bulk heterojunction (BHJ) concept have been studied extensively over the past decade due to many promising merits including low fabrication cost, light weight, high mechanical flexibility, tunable chemical and physical properties *via* molecular design, and fast module installation rate.[1–5] By controlling the morphology of the active layer, modifying the interfaces, and building tandem cells, power conversion efficiencies (PCE) beyond 9% have been demonstrated, pushing this technology closer to commercialization.[6–8] In order to fabricate OPVs in large scale, it is preferred to print a active layer using solution techniques in ambient conditions,[9–13] in an easy and fast manner.[14,15] Unfortunately, most of the optimal active layer morphologies as well as the high PCEs are achieved in an inert atmosphere, which is obviously not ideal for large scale printing processes.

Meanwhile, conjugated polymers have been the work horse donor material for high performance OPVs. A main drawback of the polymer donor material is the batch to batch variation, which often makes the solar cell performance unpredictable. On the other hand, small molecules offer great advantages in terms of ease of purification, discrete molecular weight, small batch-to-batch material and device variation, strong tendency for self-assembly and potentially high charge carrier mobility, *etc.* The challenge for solution-processed small molecule BHJ OPVs is to enhance the molecular order for better charge carrier mobility, and at the same time, to restrict the domain size due to limited exciton diffusion length. Strategies such as thermal annealing and use of solvent additives or solid additives have been reported.[16–21] It has also been realized that solvent vapor annealing (SVA), which is suitable for ambient condition processing, helps to form crystalline domains.[22–26] Solvent vapor can penetrate into the film, allowing the molecules to re-organize for a more ordered packing structure. A few groups successfully used SVA to treat the active layer and demonstrated improved OPV performance.[27–29] However, the mechanism is still not fully understood and no solvent selection rule has been identified.[30]

In this contribution, a range of solvents with different solvent properties are used to vapor-anneal the active layer, which consists of a small molecule donor, 3,6-bis(5-(benzofuran-2-yl) thiophen-2-yl)-2,5-bis(2-ethylhexyl)pyrrolo[3,4-*c*]pyrrole-1,4-dione (DPP(TBFu)$_2$),[31–36] and a common fullerene derivative, [6,6]-phenyl $C_{71}$-butyric acid methyl ester ($PC_{71}BM$). Their chemical structures are shown in Fig. 1a. It is found that SVA of only a few seconds can change the morphology drastically, which is clearly observed in transmission electron microscopy (TEM) tomography analysis. Besides short-circuit current density ($J_{sc}$) and fill factor (FF), SVA can improve the hole mobility.

Furthermore, solvents with high vapor pressure and medium solubility for the donor molecules are the ideal SVA solvent for OPV application. DPP(TBFu)$_2$:$PC_{71}BM$ films that are vapor-annealed by tetrahydrofuran (THF) or carbon disulfide ($CS_2$),

[a]School of Chemistry, Bio21 Institute, The University of Melbourne, 30 Flemington Road, Parkville, Victoria 3010, Australia. E-mail: sunkuan.stuart@gmail.com; wwhwong@unimelb.edu.au; djjones@unimelb.edu.au

[b]Advanced Microscopy Facility, Bio21 Institute, The University of Melbourne, 30 Flemington Road, Parkville, Victoria 3010, Australia

[c]Laboratory for Electron Microscopy (LEM), Karlsruhe Institute of Technology (KIT), Engesserstraße 7, Karlsruhe 76131, Germany

† Electronic supplementary information (ESI) available. See DOI: 10.1039/c4ta01125b

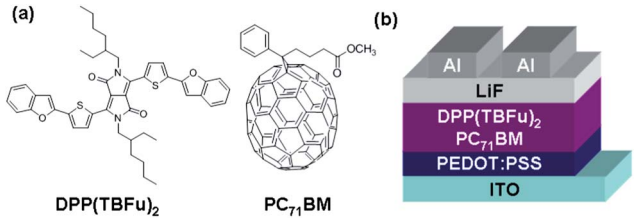


Fig. 1 (a) Chemical structure of $DPP(TBFu)_2$ donor and $PC_{71}BM$ acceptor and (b) OPV cell architecture.

produce the highest PCE of 5.2%. We note that the fabrication and treatment of the active layer are entirely done at room temperature in air, suggesting that fast SVA is potentially compatible with large scale production of OPVs.[37]

## 2. Experimental section

### 2.1 Materials & solvents

$DPP(TBFu)_2$ was synthesized by following literature methods.[31] $PC_{71}BM$ was purchased from Nano-C. All the solvents were ACS reagent grade and supplied by Sigma-Aldrich.

### 2.2 Solvent vapor annealing (SVA)

SVA was conducted in ambient conditions at room temperature. The respective vapor pressures are summarized in Table 1. Respective solvent (2 ml) was injected into a 30 mm glass Petri dish. The Petri dish was closed for 5 min to let the vapor saturate the treatment chamber. Then as-cast film was attached on the back side of a second Petri dish lid, which was quickly swapped with the lid covering the solvent-containing Petri dish. The film was about 1 cm above the solvent level during the SVA. After a certain duration, the film was removed from the treatment chamber.

### 2.3 Film characterizations

UV-vis-NIR spectra were recorded by a Varian Cary 50 Spectrometer. TEM bright field images were obtained by a FEI Tecnai TF30 TEM equipped with beam blank function. For electron tomography, tilt series were acquired using the Xplore 3D software (FEI Company). Tomograms were recorded between −65 and +65 degrees at 2° intervals and aligned with IMOD.[38] A 3D model rendering employed 3d mod software.[39] Each model was generated from the aligned tomogram. The $DPP(TBFu)_2$ donor phase was rendered in golden color, while the $PC_{71}BM$ acceptor phase was represented by empty space in ESI movies except movie 2,† in which the acceptor was rendered in green color to show the flake-like structure of $PC_{71}BM$. The scale bar is 50 nm in the model movies and 100 nm in the tomogram movies. AFM images were acquired with an Asylum Research Cypher scanning probe microscope operated in a tapping mode. To obtain hole mobility using SCLCs, hole-only devices were constructed using a cell architecture of ITO/PEDOT:PSS/$DPP(TBFu)_2$:$PC_{71}BM$/Au. Their dark currents were recorded by a computer programmed Keithley 2400 source meter and then fitted by the Mott–Gurney equation.[40,41] Film thickness was determined by a Veeco Dektak 150+ Surface Profiler.

### 2.4 OPV fabrication & characterizations

All the fabrication and characterization processes were carried out in air. Patterned ITO glasses were washed sequentially by detergent, deionized water, acetone, and 2-propanol in an ultrasonication bath and UV/ozone-treated. PEDOT:PSS (Clevios P VP AI 4083) was spin-coated at 8000 rpm and then baked at 150 °C for 10 min in air. After cooling down to room temperature, a solution comprising 8 mg $DPP(TBFu)_2$ and 5.3 mg $PC_{71}BM$ in 1 ml of chloroform was spin coated at 65 °C at 1500 rpm on top of the substrate. The films were solvent vapor annealed by respective solvent at various durations. Then they were transferred to a thermal evaporator where 1 nm LiF and 100 nm aluminum were deposited through a shadow mask (active area was 0.10 $cm^2$) at a base pressure of $1 \times 10^{-6}$ Torr. Film thicknesses were determined by a Veeco Dektak 150+ Surface Profiler. The thickness of the photoactive layers was optimized and was typically between 100 and 120 nm. The solar cells were illuminated at 100 mW $cm^{-2}$ using a 1 kW Oriel solar simulator with an AM 1.5G filter in air, and *J–V* curves were measured using a Keithley 2400 source meter. For accurate measurement, the light intensity was calibrated using a reference silicon solar cell (PV measurements Inc.) certified by the National Renewable Energy Laboratory.

Table 1 Solvent properties, OPV performance parameters and optimal treatment durations of different solvents used in solvent vapor annealing of the active layer

| Solvent | Vapor pressure 20 °C [mm Hg] | Donor solubility[a] [mg $ml^{-1}$] | Acceptor solubility[a] [mg $ml^{-1}$] | $V_{oc}$ [V] | $J_{sc}$ [mA $cm^{-2}$] | FF [%] | PCE [%] | Treatment duration [s] |
|---|---|---|---|---|---|---|---|---|
| No SVA | — | — | — | 0.95 | 2.08 | 28 | 0.55 | — |
| THF | 150 | 4.41 | 3.45 | 0.78 | 11.72 | 56 | 5.15 | 20 |
| $CS_2$ | 300 | 4.46 | 142 | 0.82 | 11.15 | 56 | 5.16 | 7 |
| CB | 9 | 3.39 | 60.6 | 0.82 | 8.29 | 55 | 3.72 | 10 |
| *o*DCB | 1.2 | 4.45 | 203 | 0.8 | 5.41 | 56 | 2.44 | 20 |
| $CHCl_3$ | 158 | 15.3 | 61.1 | 0.79 | 8.18 | 55 | 3.57 | 10 |
| Acetone | 180 | <0.5 | <0.5 | 0.81 | 10.40 | 43 | 3.64 | 120 |
| DCE | 64 | 0.59 | 3.47 | 0.83 | 10.48 | 56 | 4.85 | 25 |

[a] Solubility parameters for all solvents were adapted from ref. 42.

## 3. Results and discussion

The solvent vapor annealing was carried out by filling 2 ml of the solvent into a glass Petri dish of 30 mm in diameter. The closed Petri-dish was held in ambient conditions (22 °C) for 5 min to let the solvent vapor saturate the chamber. The as-cast DPP(TBFu)$_2$:PC$_{71}$BM film was attached at the back of the Petri dish lid and exposed to the vapor for various durations. The SVA-treated films were assembled into OPVs with a device architecture of ITO/PEDOT:PSS/DPP(TBFu)$_2$:PC$_{71}$BM/LiF/Al, as illustrated in Fig. 1b. The active layer deposition and treatment and OPV characterization were all completed in air.

Solvents with different vapor pressures, DPP(TBFu)$_2$ donor solubilities and PC$_{71}$BM acceptor solubilities were selected for SVA, including chloroform ($CHCl_3$), acetone, 1,2-dichloroethane (DCE), THF, $CS_2$, chlorobenzene (CB) and 1,2-dichlorobenzene (*o*DCB). The solvent properties,[42] photovoltaic performance parameters and optimal treatment duration are listed in Table 1. Fig. 2a displays the current density (*J*)–voltage (*V*) curves of OPVs at optimized SVA conditions. The optimization process for each solvent can be found in Fig. S1 and Table S1 in ESI.† Compared with the untreated OPV, SVA led to significant improvement in $J_{sc}$ and FF, but a slight drop in open-circuit voltage ($V_{oc}$). The overall effect was a more than fourfold enhancement in PCE. The best photovoltaic performance was achieved by using THF or $CS_2$ vapors, with $V_{oc}$ around 0.8 V, $J_{sc}$ above 11 mA cm$^{-2}$, high FF of 0.56 and PCE of 5.2%. The results were reproducible within two material batches and five device batches by two researchers (Fig. S2 and Table S2, ESI†). Both THF and $CS_2$ have high vapor pressure, and the donor material DPP(TBFu)$_2$ has medium solubility in both solvents. Interestingly however, PC$_{71}$BM exhibits much better solubility in $CS_2$ (142 mg ml$^{-1}$) compared with THF (3.45 mg ml$^{-1}$). These results suggest that the combination of high vapor pressure and medium solubility of the donor material implies fast vapor penetration into the active layer, moderate solvent–solid interaction and rapid dissipation of the solvent vapor after the treatment, all of which we believe play critical roles in SVA for OPV application. On the other hand, the acceptor solubility appears to have little effect on the photovoltaic performance, and thus is not important in SVA treatment.

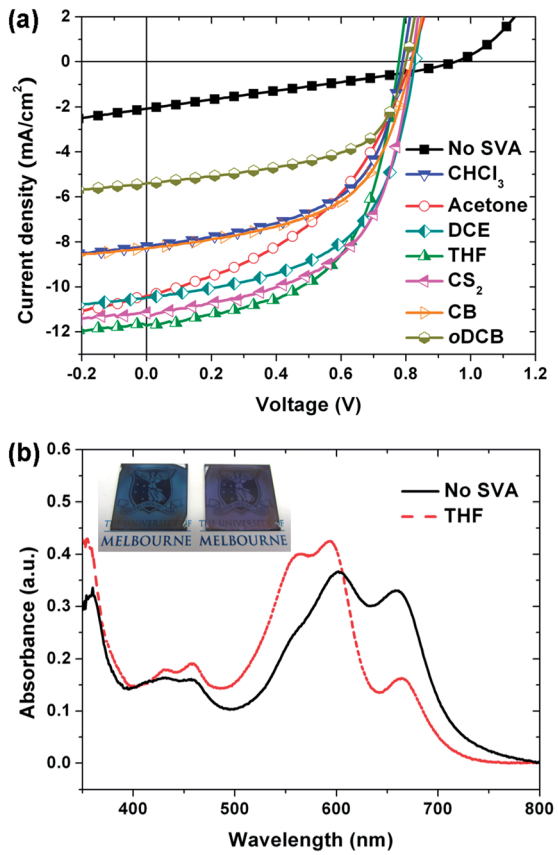


Fig. 2 (a) Current density–voltage (*J*–*V*) curves of DPP(TBFu)$_2$:PC$_{71}$BM-based OPVs without and with solvent vapor annealing (SVA) by different solvents. (b) UV-Vis-NIR spectra of DPP(TBFu)$_2$:PC$_{71}$BM blend films without and with SVA by THF for 20 s. Inset of (b) shows digital pictures of the films before (left) and after (right) the treatment.

Further evidence for this hypothesis was obtained when solvents with similar DPP(TBFu)$_2$ solubility but low vapor pressure, such as CB and *o*DCB, were tested for SVA. With decreasing vapor pressure, $V_{oc}$ and FF remained almost constant while $J_{sc}$ was reduced. Likely, the low vapor pressure solvent vapors remained inside the films for a much longer duration even after the films were removed from the treatment chamber, which caused over-growth of the donor crystals.[43] Solvents with high vapor pressure but different DPP(TBFu)$_2$ solubilities were also investigated. DPP(TBFu)$_2$ has the highest solubility in $CHCl_3$ (15.3 mg ml$^{-1}$), followed by DCE (0.59 mg ml$^{-1}$) and is least soluble in acetone (<0.5 mg ml$^{-1}$). Table 1 suggests that too high or too low solubility does not produce good OPV performance. Donor solubilities in the range between 0.5 and 5 mg ml$^{-1}$ are suitable. Presumably, solvents of high donor solubility result in fast donor crystal growth, leading to large average domain size and wide domain size distribution. In contrast, solvents of low donor solubility can hardly dissolve the donor phase and then penetrate into the film. In fact, the optimum treatment duration for acetone SVA is much longer than that for any other solvent (Table 1), which we attribute to a much slower film penetration and diffusion rate.

The SVA process can be monitored by color change of the DPP(TBFu)$_2$:PC$_{71}$BM film. Fig. 2b shows the respective UV-Vis-NIR spectra and digital images of the films before and after THF SVA for 20 s. Upon exposure to these vapors, the film color changed from dark green to purple (inset of Fig. 2b). The absorption profile changed drastically as well. Due to aggregation of the DPP(TBFu)$_2$ molecules, the spectrum was blue-shifted after SVA. The intensity of the peak at 660 nm was reduced, while those at 595 and 560 nm were enhanced. The intensity ratio between the peak at 595 nm and that at 660 nm increased from 1.1 to 2.6 after the treatment. SVA by other solvents induced similar changes in the absorption profile (Fig. S3, ESI†). We attribute the change in the absorption spectrum to changes in the molecular order and/or inter-molecular interaction, as it was described in the literature for DPP material systems previously.[31] A similar phenomenon was observed for

 

the same material system after thermal annealing and dichloromethane vapor annealing by other research groups. Such a change in the absorption profile was related to improved crystallinity of the DPP(TBFu)$_2$ donor phase, as suggested by their XRD results.[30,31]

The SVA influence on the morphology of the DPP(TBFu)$_2$:PC$_{71}$BM blend film was studied by transmission electron microscopy (TEM) and tomography, which is the most relevant technique to study the morphology in three dimensions, but has been rarely employed in OPV research,[44–47] especially in small molecule-based OPVs.[48] Fig. 3 shows the TEM bright field images and 3D computer models of the films before and after SVA by different solvents at their best OPV performance. The video clips of the tomograms and constructed models can be found in the ESI movies.† Before SVA treatment, TEM bright field images (Fig. 3a) showed a few dark structures homogeneously distributed in the bright background. Its angle-tilt tomogram suggested that the dark structures were flakes that were embedded inside the film and occasionally protruded out of the front surface (Fig. 3i and ESI movie 1 & 2†). Since PC$_{71}$BM is denser than DPP(TBFu)$_2$, the dark phases can be interpreted as PC$_{71}$BM acceptors, which form very large aggregates.[49] After SVA treatment, the film morphology changed considerably. Fig. 3b–h shows that fiber-like structures appear in the films upon SVA. These fiber-like structures can be attributed to DPP(TBFu)$_2$ crystallites. Different solvents resulted in DPP(TBFu)$_2$ crystalline fibers of different sizes, with $CHCl_3$, CB and *o*DCB producing bigger fibers (Fig. 3b, g and h), while acetone, DCE, THF and $CS_2$ produced much finer fibers (Fig. 3c–f). This observation was further confirmed by tomography and 3D models (Fig. S4† and 3j–l). The difference in fiber size is mainly determined by the solvent–DPP(TBFu)$_2$ interaction strength and duration, which are governed by solvent vapor pressure and DPP(TBFu)$_2$ solubility.

The surface texture and roughness were examined by tapping-mode atomic force microscopy (AFM) to gather additional information on the morphology change induced by SVA. Fig. 4a–h depicts the AFM topographic images of the DPP(TBFu)$_2$:PC$_{71}$BM blend film before and after SVA by different solvents. Without SVA (Fig. 4a), large parts of the film

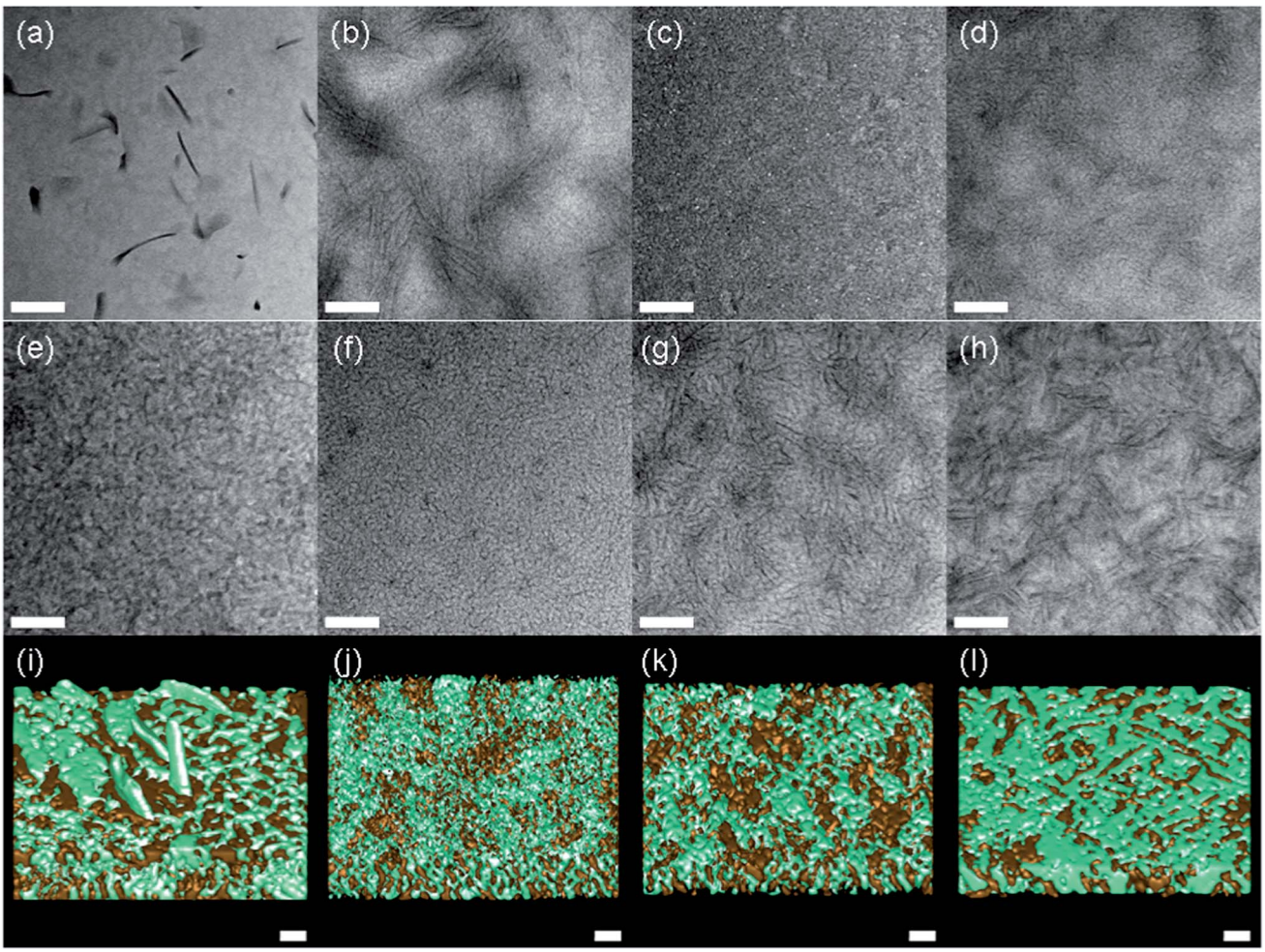


Fig. 3 (a–h) TEM bright field images of DPP(TBFu)$_2$:PC$_{71}$BM blend film (a) before and after SVA by (b) $CHCl_3$, (c) acetone, (d) DCE, (e) THF, (f) $CS_2$, (g) CB and (h) *o*DCB. The scale bar is 200 nm. The defocusing is typically between 3 and 5 μm. (i–l) Reconstructed 3D models from the tomograms of thin films (i) before and after SVA by (j) acetone, (k) $CS_2$ and (l) *o*DCB. DPP(TBFu)$_2$ donor phase is rendered in golden color while PC$_{71}$BM acceptor phase is rendered in green. The scale bar is 50 nm.

surface were smooth and featureless with a root-mean-square roughness ($R_{rms}$) of 0.39 nm, which was in good agreement with a previous report.[31] SVA induced significant changes to the surface texture, with visible fiber-like structures and an increase in $R_{rms}$. Films treated by $CHCl_3$, CB and *o*DCB (Fig. 4b, g and h) exhibited extremely large domains ranging between 50 and 300 nm. The $R_{rms}$ values of the three films were all above 3 nm. Domain sizes larger than 50 nm are detrimental to charge carrier generation due to the limited exciton diffusion length. This result explains the reduced $J_{sc}$ observed in $CHCl_3$-, CB- and *o*DCB-treated OPVs. Films treated by acetone, DCE, THF and $CS_2$ exhibited smaller domain sizes of approximately 20–50 nm. These observations were consistent with the TEM and tomography results. The $R_{rms}$ values of these films were between 1.4 and 2.7 nm, which agrees well with the optimal roughness determined by other groups.[30,31] We note that due to limited donor solubility and much longer treatment duration, acetone-treated films showed a large number of well-defined DPP(TBFu)$_2$ crystalline fibers on the front surface of the film (Fig. 4c). On the other hand, TEM tomograms revealed $PC_{71}BM$, *i.e.*, dark elongated structures indicated by arrows in Fig. 4j, aggregating at the bottom of the film. In comparison, donor and acceptor phases were distributed more homogenously in $CS_2$-treated films (Fig. 4k and l). Any accumulation of donor material at the cathode interface or acceptor material near the anode would increase the bimolecular recombination rate, which may be the reason for the observed low FF in acetone-treated OPV devices but will require further investigation in the future.[32,50,51]

We note that our best solvent annealed solar cells outperformed the thermally annealed devices that were reported in the literature before.[36] To enable direct comparison, we thermally annealed DPP(TBFu)$_2$:PC71BM layers that were fabricated under the same conditions. This thermal annealing also changed the absorption profile and surface texture of the active layer (Fig. S5 and S6†), yielding device power conversion efficiencies of 3.8% upon annealing in inert atmosphere and 2.2% upon annealing in air (Fig. S7†).

Finally, the hole mobility of donor–acceptor blend films was determined from the space charge limited currents (SCLC) (Fig. S8 and Table S3†). The as-cast film showed a hole mobility of $2 \times 10^{-4}$ $cm^2$ ($V^{-1}$ $s^{-1}$). SVA improved the hole mobility, but thermal annealing did not, which was consistent with a

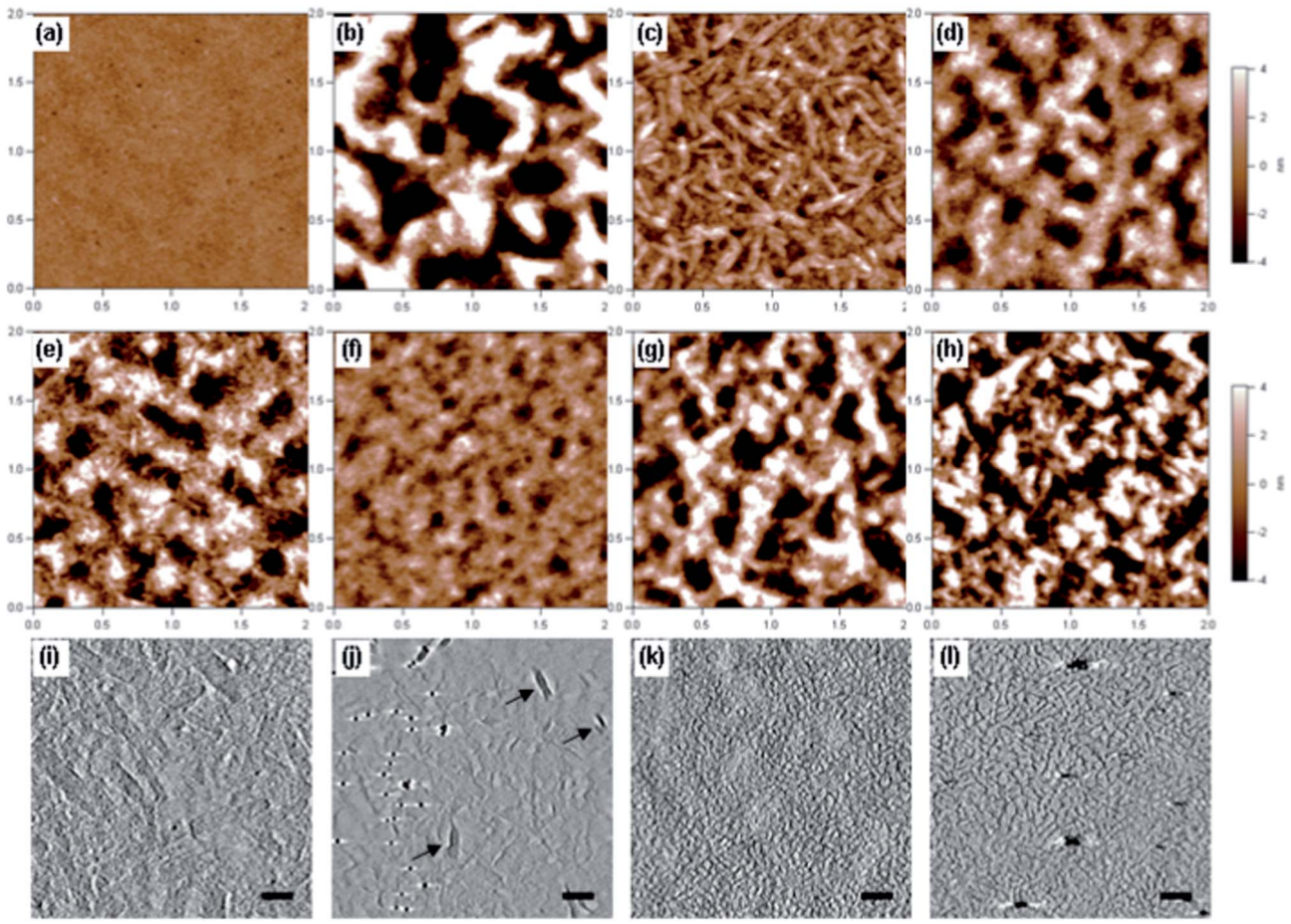


Fig. 4 (a–h) AFM topographic images of DPP(TBFu)$_2$:$PC_{71}BM$ blend film (a) before and after SVA by (b) $CHCl_3$, (c) acetone, (d) DCE, (e) THF, (f) $CS_2$, (g) CB and (h) *o*DCB. The root-mean-square roughness of the films is (a) 0.39, (b) 4.75, (c) 1.50, (d) 2.28, (e) 2.72, (f) 1.39, (g) 3.28, and (h) 3.83 nm, respectively. The scale is 2 × 2 μm and height bar is 8 nm. (i–l) Slides of TEM tomograms of films treated by (i and j) acetone and (k and l) $CS_2$. (i) and (k) are the top surface in contact with LiF/Al cathode while (j) and (l) show the bottom surface in contact with PEDOT:PSS/ITO anode. The scale bar is 100 nm. The arrows in (j) indicate the presence of $PC_{71}BM$ phase on the bottom surface.

 

previous report.[31] More specifically, SVA almost tripled the hole mobility to 5–7 $\times$ $10^{-4}$ $cm^2$ $V^{-1}$ $s^{-1}$. We attribute the improved mobility to a more ordered donor phase after SVA, enabling the observed enhancement in $J_{sc}$ and FF.

## 4. Conclusions

In summary, a solvent vapor annealing (SVA) method was demonstrated to improve the photovoltaic performance of DPP(TBFu)$_2$:$PC_{71}BM$-based OPVs through changes in blend film morphology that were revealed in 3D by TEM tomography. A range of solvents were tested and compared. Solvents with high vapor pressure and medium donor solubility were found to produce changes in morphology leading to higher solar cell efficiency, while acceptor solubility in these solvents played an insignificant role in determining the photovoltaic performance. The best efficiencies were achieved by SVA using THF or $CS_2$, both yielding a PCE of 5.2%, which was the highest PCE for the DPP(TBFu)$_2$:$PC_{71}BM$ material combination. To the best of our knowledge, this is the first demonstration of highly efficient, air-processed small molecule OPVs and is comparable with the best polymer-based OPVs fabricated in air.[52–56] As the treatment is rapid and takes place in ambient conditions, it has great potential to be incorporated into large-scale continuous OPV fabrication processes.

## Acknowledgements

We thank Australian Renewable Energy Agency (ARENA) for supporting this work through the Australia–Germany Research Exchange Project Grant (1-GER001) and the Victorian Organic Solar Cell consortium (VICOSC) with funding provided by the Victorian State Government Department of Primary Industries (Energy Technology Innovation Strategy), the Victorian State Government Department of Business Innovation (Victorian Science Agenda) and ARENA (Project 2-A018). W. W. H. Wong thanks the fellowship sponsored by ARENA. The authors are grateful to Prof. Andrew B. Holmes at the University of Melbourne and Dr Alexander Colsmann at the Karlsruhe Institute of Technology for in-depth discussions and kind support.

## Notes and references

1 A. W. Hains, Z. Q. Liang, M. A. Woodhouse and B. A. Gregg, *Chem. Rev.*, 2010, **110**, 6689–6735.
2 A. Mishra and P. Bäuerle, *Angew. Chem., Int. Ed.*, 2012, **51**, 2020–2067.
3 Y. F. Li, *Acc. Chem. Res.*, 2012, **45**, 723–733.
4 L. Dou, J. You, Z. Hong, Z. Xu, G. Li, R. A. Street and Y. Yang, *Adv. Mater.*, 2013, **25**, 6642–6671.
5 F. C. Krebs, N. Espinosa, M. Hösel, R. R. Søndergaard and M. Jørgensen, *Adv. Mater.*, 2014, **26**, 29–39.
6 Z. He, C. Zhong, S. Su, M. Xu, H. Wu and Y. Cao, *Nat. Photonics*, 2012, **6**, 591–595.
7 J. You, C.-C. Chen, Z. Hong, K. Yoshimura, K. Ohya, R. Xu, S. Ye, J. Gao, G. Li and Y. Yang, *Adv. Mater.*, 2013, **25**, 3973–3978.
8 J. You, L. Dou, K. Yoshimura, T. Kato, K. Ohya, T. Moriarty, K. Emery, C.-C. Chen, J. Gao, G. Li and Y. Yang, *Nat. Commun.*, 2013, **4**, 1446.
9 F. C. Krebs, *Sol. Energy Mater. Sol. Cells*, 2009, **93**, 394–412.
10 F. C. Krebs, *Org. Electron.*, 2009, **10**, 761–768.
11 F. C. Krebs, *Sol. Energy Mater. Sol. Cells*, 2009, **93**, 465–475.
12 F. C. Krebs, M. Jorgensen, K. Norrman, O. Hagemann, J. Alstrup, T. D. Nielsen, J. Fyenbo, K. Larsen and J. Kristensen, *Sol. Energy Mater. Sol. Cells*, 2009, **93**, 422–441.
13 W. Gaynor, J. Y. Lee and P. Peumans, *ACS Nano*, 2010, **4**, 30–34.
14 H. J. Park, M.-G. Kang, S. H. Ahn and L. J. Guo, *Adv. Mater.*, 2010, **22**, E247–E253.
15 J. Y. Oh, M. Shin, T. I. Lee, W. S. Jang, Y.-J. Lee, C. S. Kim, J.-W. Kang, J.-M. Myoung, H. K. Baik and U. Jeong, *Macromolecules*, 2013, **46**, 3534–3543.
16 W. Shin, T. Yasuda, G. Watanabe, Y. S. Yang and C. Adachi, *Chem. Mater.*, 2013, **25**, 2549–2556.
17 K. R. Graham, R. Stalder, P. M. Wieruszewski, D. G. Patel, D. H. Salazar and J. R. Reynolds, *ACS Appl. Mater. Interfaces*, 2013, **5**, 63–71.
18 J. Huang, C. Zhan, X. Zhang, Y. Zhao, Z. Lu, H. Jia, B. Jiang, J. Ye, S. Zhang, A. Tang, Y. Liu, Q. Pei and J. Yao, *ACS Appl. Mater. Interfaces*, 2013, **5**, 2033–2039.
19 H. Wang, F. Liu, L. Bu, J. Gao, C. Wang, W. Wei and T. P. Russell, *Adv. Mater.*, 2013, **25**, 6519–6525.
20 K. R. Graham, P. M. Wieruszewski, R. Stalder, M. J. Hartel, J. Mei, F. So and J. R. Reynolds, *Adv. Funct. Mater.*, 2012, **22**, 4801–4813.
21 J. Zhou, X. Wan, Y. Liu, Y. Zuo, Z. Li, G. He, G. Long, W. Ni, C. Li, X. Su and Y. Chen, *J. Am. Chem. Soc.*, 2012, **134**, 16345–16351.
22 B. A. Gregg, *J. Phys. Chem.*, 1996, **100**, 852–859.
23 K. C. Dickey, J. E. Anthony and Y. L. Loo, *Adv. Mater.*, 2006, **18**, 1721–1726.
24 M. T. Lloyd, A. C. Mayer, S. Subramanian, D. A. Mourey, D. J. Herman, A. V. Bapat, J. E. Anthony and G. G. Malliaras, *J. Am. Chem. Soc.*, 2007, **129**, 9144–9149.
25 G. H. Lu, L. G. Li and X. N. Yang, *Adv. Mater.*, 2007, **19**, 3594–3598.
26 J. Vogelsang, J. Brazard, T. Adachi, J. C. Bolinger and P. F. Barbara, *Angew. Chem., Int. Ed.*, 2011, **50**, 2257–2261.
27 Y. Zhao, Z. Xie, Y. Qu, Y. Geng and L. Wang, *Appl. Phys. Lett.*, 2007, **90**, 043504.
28 H. Tang, G. Lu, L. Li, J. Li, Y. Wang and X. Yang, *J. Mater. Chem.*, 2010, **20**, 683–688.
29 G. Wei, S. Wang, K. Sun, M. E. Thompson and S. R. Forrest, *Adv. Energy Mater.*, 2011, **1**, 184–187.
30 A. Viterisi, F. Gispert-Guirado, J. W. Ryan and E. Palomares, *J. Mater. Chem.*, 2012, **22**, 15175–15182.
31 B. Walker, A. B. Tamayo, X.-D. Dang, P. Zalar, J. H. Seo, A. Garcia, M. Tantiwiwat and T.-Q. Nguyen, *Adv. Funct. Mater.*, 2009, **19**, 3063–3069.

32 Y. Zhang, X.-D. Dang, C. Kim and T.-Q. Nguyen, *Adv. Energy Mater.*, 2011, **1**, 610–617.
33 J. Liu, Y. Zhang, H. Phan, A. Sharenko, P. Moonsin, B. Walker, V. Promarak and T.-Q. Nguyen, *Adv. Mater.*, 2013, **25**, 3645–3650.
34 Z. Li, X. Zhang, Y. Zhang, C. F. Woellner, M. Kuik, J. Liu, T.-Q. Nguyen and G. Lu, *J. Phys. Chem. C*, 2013, **117**, 6730–6740.
35 X.-D. Dang, A. B. Tamayo, J. Seo, C. V. Hoven, B. Walker and T.-Q. Nguyen, *Adv. Funct. Mater.*, 2010, **20**, 3314–3321.
36 J. Liu, B. Walker, A. Tamayo, Y. Zhang and T.-Q. Nguyen, *Adv. Funct. Mater.*, 2013, **23**, 47–56.
37 Y. Lin, H. F. Dam, T. R. Andersen, E. Bundgaard, W. Fu, H. Chen, F. C. Krebs and X. Zhan, *J. Mater. Chem. C*, 2013, **1**, 8007–8010.
38 J. R. Kremer, D. N. Mastronarde and J. R. McIntosh, *J. Struct. Biol.*, 1996, **116**, 71–76.
39 http://bio3d.colorado.edu/.
40 V. D. Mihailetchi, J. K. J. van Duren, P. W. M. Blom, J. C. Hummelen, R. A. J. Janssen, J. M. Kroon, M. T. Rispens, W. J. H. Verhees and M. M. Wienk, *Adv. Funct. Mater.*, 2003, **13**, 43–46.
41 V. D. Mihailetchi, J. Wildeman and P. W. M. Blom, *Phys. Rev. Lett.*, 2005, **94**, 126602.
42 B. Walker, A. Tamayo, D. T. Duong, X.-D. Dang, C. Kim, J. Granstrom and T.-Q. Nguyen, *Adv. Energy Mater.*, 2011, **1**, 221–229.
43 L. Chang, H. W. A. Lademann, J.-B. Bonekamp, K. Meerholz and A. J. Moulé, *Adv. Funct. Mater.*, 2011, **21**, 1779–1787.
44 S. S. van Bavel, E. Sourty, G. de With and J. Loos, *Nano Lett.*, 2009, **9**, 507–513.
45 A. A. Herzing, L. J. Richter and I. M. Anderson, *J. Phys. Chem. C*, 2010, **114**, 17501–17508.
46 M. Kim, J.-H. Kim, H. H. Choi, J. H. Park, S. B. Jo, M. Sim, J. S. Kim, H. Jinnai, Y. D. Park and K. Cho, *Adv. Energy Mater.*, 2014, DOI: 10.1002/aenm.201300612.
47 J. D. Roehling, K. J. Batenburg, F. B. Swain, A. J. Moulé and I. Arslan, *Adv. Funct. Mater.*, 2013, **23**, 2115–2122.
48 M. Pfaff, P. Müller, P. Bockstaller, E. Müller, J. Subbiah, W. W. H. Wong, M. F. G. Klein, A. Kiersnowski, S. R. Puniredd, W. Pisula, A. Colsmann, D. Gerthsen and D. J. Jones, *ACS Appl. Mater. Interfaces*, 2013, **5**, 11554–11562.
49 S. S. van Bavel, M. Bärenklau, G. de With, H. Hoppe and J. Loos, *Adv. Funct. Mater.*, 2010, **20**, 1458–1463.
50 L. J. A. Koster, V. D. Mihailetchi and P. W. M. Blom, *Appl. Phys. Lett.*, 2006, **88**, 052104.
51 M.-S. Kim, B.-G. Kim and J. Kim, *ACS Appl. Mater. Interfaces*, 2009, **1**, 1264–1269.
52 C. Y. Nam, D. Su and C. T. Black, *Adv. Funct. Mater.*, 2009, **19**, 3552–3559.
53 S. J. Wu, J. H. Li, Q. D. Tai and F. Yan, *J. Phys. Chem. C*, 2010, **114**, 21873–21877.
54 Z. Y. Hu, J. J. Zhang, S. Z. Xiong and Y. Zhao, *Org. Electron.*, 2012, **13**, 142–146.
55 Z. Y. Hu, J. J. Zhang and Y. J. Zhu, *Appl. Phys. Lett.*, 2013, **102**, 043307.
56 E. S. R. Bovill, J. Griffin, T. Wang, J. W. Kingsley, H. Yi, A. Iraqi, A. R. Buckley and D. G. Lidzey, *Appl. Phys. Lett.*, 2013, **102**, 183303.